In situ study of oxidation states of platinum nanoparticles on a polymer electrolyte fuel cell electrode by near ambient pressure hard X-ray photoelectron spectroscopy

doi: 10.1039/C6CP06634H

In situ study of oxidation states of platinum nanoparticles on a polymer electrolyte fuel cell electrode by near ambient pressure hard X-ray photoelectron spectroscopy

Yasumasa Takagi,*[a,b] Heng Wang,[a‡] Yohei Uemura,[a,b] Takahiro Nakamura,[a] Liwei Yu,[a] Oki Sekizawa,[c] Tomoya Uruga,[c,d] Mizuki Tada,[e] Gabor Samjeskè,[c] Yasuhiro Iwasawa,[c] and Toshihiko Yokoyama[a,b]

Abstract

We performed *in situ* hard X-ray photoelectron spectroscopy (HAXPES) measurements of the electronic states of platinum nanoparticles on the cathode electrocatalyst of a polymer electrolyte fuel cell (PEFC) using a near ambient pressure (NAP) HAXPES instrument having an 8 keV excitation source. We successfully observed *in situ* NAP-HAXPES spectra for the Pt/C cathode catalysts of PEFC under working conditions involving water, not only for the Pt 3d states with large photoionization cross sections in the hard X-ray regime but also for the Pt 4f states and valence band with small photoionization cross sections. Thus, this setup allowed *in situ* observation of a variety of hard PEFC systems under operating conditions. The Pt 4f spectra of the Pt/C electrocatalysts in PEFCs clearly showed peaks originating from oxidized Pt(II) at 1.4 V, which unambiguously shows that Pt(IV) species do not exist on the Pt nanoparticles even at such large positive voltages. The water oxidation reaction might take place at that potential (the standard potential of 1.23 V versus a standard hydrogen electrode) but such a reaction should not lead to a buildup of detectable Pt(IV) species. The voltage-dependent NAP-HAXPES Pt 3d spectra revealed different behaviors when increasing voltage (0.6 → 1.0 V) compared with decreasing voltage (1.0 → 0.6 V), showing a clear hysteresis. Moreover, quantitative peak-fitting analysis showed that the fraction of non-metallic Pt species matched the ratio of surface to total Pt atoms in the nanoparticles, which suggests that Pt oxidation only takes place at the surface of the Pt nanoparticles on the PEFC cathode, and the inner Pt atoms do not participate in the reaction. In the valence band spectra, the density of

electronic states near the Fermi edge reduces with decreasing particle size, indicating an increase in the electrocatalytic activity. Additionally, a change in the valence band structure due to the oxidation of platinum atoms was also observed at large positive voltages. The developed apparatus is a valuable *in situ* tool for the investigation of the electronic states of PEFC electrocatalysts under working conditions.

---

[a] Department of Materials Molecular Science, Institute for Molecular Science, Okazaki, Aichi 444-8585, Japan, E-mail: *ytakagi@ims.ac.jp*

[b] SOKENDAI (The Graduate University for Advanced Studies), Okazaki, Aichi 444-8585, Japan.

[c] Innovation Research Center for Fuel Cells, The University of Electro-Communications, Chofu, Tokyo 182-8585, Japan.

[d] Japan Synchrotron Radiation Research Institute, SPring-8, Sayo, Hyogo 679-5198, Japan.

[e] Research Center for Materials Science, Nagoya University, Nagoya, Aichi 464-8602, Japan.

[‡] Present address: School of Material and Chemical Engineering, Zhengzhou University of Light Industry, Zhengzhou Henan Province, 450001, China.

[†] Electronic supplementary information (ESI) available.

1 Introduction

Polymer electrolyte fuel cells (PEFCs) are one of the most promising next-generation automotive power sources. Platinum nanoparticles (NPs) on carbon supports are generally used in PEFCs as the highest efficiency catalyst. Since their durability is a key factor for their practical use, approaches for improving their durability, particularly for the cathode electrocatalysts in PEFCs, have been extensively investigated by many researchers.[1-4] In these studies, it is important to observe directly the oxidation states of the cathode Pt NPs at large positive voltages, because the severe oxidation, dissolution, and sintering of Pt NPs occur at the cathode in addition to carbon corrosion when more positive voltages are applied to the PEFC cathode, for instance, during startup/shutdown operations.

In situ observations of PEFCs have been made using several methods, such as Fourier transform infrared spectroscopy,[5] X-ray absorption fine structure (XAFS),[6,7] X-ray photoelectron spectroscopy (XPS),[8-10] X-ray emission spectroscopy,[11] and transmission electron microscopy.[12-14] Recently, *in situ* XAFS measurements of PEFC electrodes have revealed restructuring of the surface through observation of the Pt oxidation states and coordination numbers of Pt-O and Pt-Pt bonds in the Pt NPs at the cathode during voltage-stepping processes.[14-19] XPS provides information complementary to that obtained by XAFS. Here chemical species with different valences can be detected as separated peaks with chemical shifts,[20] and the average valence of Pt atoms in the NPs is estimated from the white line intensity of the Pt L_3-edge XAFS spectra. Moreover, the concentration of each chemical state can more easily be estimated from the ratios between peak areas in XPS spectra. In particular, in cases where more than three oxidation states of the atoms of interest may exist, XPS provides the concentration of each component, whereas the XAFS technique provides only averaged information on the oxidation states of each species in the sample.

Conventional XPS requires high vacuum conditions and only allows us to perform *ex situ*

measurements of dry samples of PEFC catalysts before and after operation. Recently, XPS systems for making measurements under ambient pressure conditions have been developed by using a differential pumping type analyzer and intense X-rays from third-generation synchrotron radiation sources. This technique is known as near ambient pressure X-ray photoelectron spectroscopy (NAP-XPS).[21-28] NAP-XPS using soft X-rays (~1 keV) can be employed for solid/gas interface measurements because the photoelectrons generated with low kinetic energy are surface sensitive.[29-31] Probing of the solid/liquid interface has been successfully achieved by using hard X-rays (≥4 keV).[32-35] In the PEFC electrode, Pt NPs are surrounded by ionomers and carbon supports and, moreover, a large amount of water exists at the working electrode of the PEFC to enhance the proton mobility. Therefore, X-ray sources with high photon energies are required for *in situ* observation of the PEFC electrode because high-energy photoelectrons are required to pass through the intermediate materials. It follows that, NAP-XPS using hard X-rays (NAP-HAXPES) should be a useful tool for the direct observation of PEFC electrodes under operating conditions.

Another advantage of using hard X-rays for such studies is that the relevant spectra, from the valence band to deep core shells, can be measured in each case depending on the purpose. The valence-band electronic states are strongly related to the activity of catalysts, whereas the chemical states of the atom of interest are directly distinguished by measuring the core-shell peaks, which do not overlap with other features. The *in situ* observation of NAP-HAXPES for the electrocatalysts in PEFCs under different applied voltages can reveal the oxidation mechanism of the catalysts at the cathode.

Recently, we reported *in situ* NAP-HAXPES measurements of Pt 3d spectra for Pt NP cathode catalysts in PEFCs under applied voltages and successfully observed the Pt oxidation of PEFC Pt/C cathodes.[33] It was, however, difficult to identify the valence of the oxidized Pt clearly, such as whether the chemical state of the oxidized Pt was divalent or tetravalent.

Moreover, the previous signal-to-noise (S/N) ratio was not high enough to discuss in detail the chemical states of the Pt NPs in the PEFC cathode catalyst.

In the present work, we have improved the focus of the incident X-rays to collect more intense photoelectron signals and have controlled more precisely the vapor pressure of water around the cathode in the PEFC to stabilize the thickness of the water layer on the Pt NP catalysts. These improvements allow us to measure the spectra from the electronic levels with low photoionization cross sections using 8 keV X-rays. We have successfully observed the Pt 4f and valence band spectra, as well as the much more intense Pt 3d spectra. The Pt 4f spectra for the Pt NP cathode catalyst at 1.4 V showed a clear peak, which originates from Pt(II) rather than Pt(IV), indicating that Pt(IV) species do not exist on the Pt NP surface even at large positive voltages. The Pt 3d spectra have been measured in detail by varying the applied voltage, and the component arising from oxidized Pt atoms was found to appear at >1.0 V with obvious hysteresis in its intensity depending on the voltage. The concentrations of the three observed Pt chemical states were estimated from the area ratios of the corresponding peaks by fitting the Pt 3d spectra. Based on a comparison of the results obtained for NPs with different particle sizes, it is concluded that the Pt oxidation only takes place at the surface of the Pt NPs at the PEFC cathode. The valence band spectra have also been successfully recorded, and the density of electronic states in the vicinity of the Fermi edge was found to reduce with decreasing particle size, indicating a higher activity for Pt NPs with smaller particle sizes. A change in the valence band structure due to Pt oxidation was also observed at large positive voltages.

2 Experimental

2.1 NAP-HAXPES measurement system and membrane electrode assembly

The *in situ* XPS measurements were conducted at the BL36XU beamline [36,37] in SPring-8, which we constructed for fuel cell catalysis research using the NAP-HAXPES system with a

commercial differential-pumping type analyzer (R4000 HiPP-2, Scienta Omicron Inc.).[38] Detailed descriptions of the measurement system and the PEFC-type measurement cells can be found in our previous report.[33] The incident photon energy was set at 7.94 keV. In order to enhance the photoelectron intensities, the crystal monochromators and focusing mirrors were precisely adjusted and an X-ray spot size at the measurement position of 20 μm (vertical) × 20 μm (horizontal) was consequently achieved by the focusing mirrors, which is six times smaller than the size of 120 μm (vertical) × 20 μm (horizontal) used in our previous study.[33] In order to avoid possible sample damages by the focused X-ray beam, the sample was scanned during the *in situ* NAP-HAXPES measurements. The gas pressure in the analysis chamber was measured with a capacitance gauge more precisely than in our previous work. In the present, experiments hydrogen gas (99.99999% purity) was supplied to the anode at a flow rate of 15 ml/min, and only water vapor was provided to the cathode from a water bath at 50 °C with the pressure controlled more accurately than before using a variable leak valve between the chamber and the water bath. The precise control of the water vapor pressure is essential for maintaining the thickness of water layers on the Pt NPs for stable photoelectron intensities. The cell voltage between the anode and cathode was controlled by a potentiostat (600E, CH Instruments, USA) and the cathode electrode was always grounded for the NAP-HAXPES measurements. In the present electrochemical setup for the NAP-HAXPES measurements, the anode was used as both the counter and reference electrodes since in the Pt/H_2 system the electrode potential does not change over a wide range of current densities. All potentials are reported with respect to the anode and were regulated by the potentiostat system shown in the ESI†. Therefore, in this study potentials are V vs RE/CE.

We used Pt NPs with two different sizes (TEC10E50E and TEC10E50E-HT; Tanaka Kikinzoku Kogyo Co., Ltd.; Pt 50 wt.%) as cathode catalysts and TEC10E50E was also used at the anode electrode. The average diameters of the Pt nanoparticles in TEC10E50E and

TEC10E50E-HT are 2.6 and 4.8 nm, respectively.[39-41] These catalysts were coated onto a membrane electrode assembly (MEA) containing a Nafion membrane (Eiwa Co. Ltd.; 5 × 5 mm^2) with cathode Pt loadings of 0.1 mg/cm^2 and 0.3 mg/cm^2 for TEC10E50E and TEC10E50E-HT, respectively, and 0.5 mg/cm^2 for the anode TEC10E50E. The MEA samples were always aged prior to the measurements.

2.2 Optimizing vapor pressure.

Cyclic voltammograms (CVs) for MEAs coated with Pt/C (TEC10E50E) under different water vapor pressures at the cathode were recorded in the potential range from 0.15 V to 1.2 V at a scan rate of 20 mV/s at room temperature (RT), as shown in Figure 1(a). Figure 1(b) shows the corresponding *in situ* HAXPES Pt $3d_{5/2}$ peaks at the cathode. The CV curves were changed with increasing water vapor pressures to be saturated at ≥4,000 Pa (Figure 1(a)). The intensity of the Pt $3d_{5/2}$ peaks decreased with increasing water vapor pressure due to inelastic photoelectron scattering from gaseous water molecules located between the sample and the electron energy analyzer, and also from the liquid water layer covering the Pt NPs at the cathode. However, except for the S/N ratio, the shape of the normalized HAXPES peaks after background subtraction did not change significantly up to 4,700 Pa. Considering the results of the proton mobility and the attenuation of the photoelectron signals in Figure 1, the most suitable water vapor pressure for the HAXPES measurement of Pt NPs in the MEA can be estimated to be around 4,000 Pa. The water vapor pressure was kept constant during the NAP-HAXPES measurement by controlling the flow and pumping rates of the water vapor. Under this pressure condition, there are few changes in the CV curves before and after the *in situ* NAP-HAXPES measurements (Figure S2, ESI†), indicating that the HAXPES measurement does not significantly change the electrochemically active surface.

The thickness of the liquid water layers on the Pt NPs in the MEA can be roughly

estimated from the decay of the HAXPES signal intensity. The effective path length through the gaseous region in this apparatus is 0.315 mm,[33,42] the total photoelectron scattering cross section of a water molecule is 4.5×10^{-17} cm^2 at an electron energy of 5.0 keV [43], and the inelastic mean free path of photoelectrons at the same energy in liquid water is 18 nm.[44] As shown in Figure 1(c), the signal attenuation with respect to that at 300 Pa is estimated to be 18% at 4,000 Pa. By using these values, the thickness of the water layer was calculated to be about 6 nm at 4,000 Pa. As the kinetic energy of the Pt $3d_{5/2}$ photoelectrons was 5.8 keV in these measurements for an excitation energy of 7.94 keV, the actual thickness of the liquid water layer is regarded to be slightly larger than the estimated value.

3 Results and discussion

Oxidation of the Pt NP catalysts occurs when a large positive voltage is applied between the electrodes. As indicated by the CV curves, the threshold voltage is approximately 0.8 V. We used *in situ* NAP-HAXPES to determine the oxidation states of the Pt NPs at the cathode at positive voltages and sufficient humidity. Figure 2 shows the Pt 4f HAXPES spectra for Pt/C (TEC10E50E) at 0.4 V and 1.4 V, which correspond to reduced and oxidized Pt states, respectively. Approximately 90 min were required to record each spectrum. The spectrum of the Pt foil at hv = 7.94 keV in high vacuum is also given in Figure 2 for comparison. The binding energies of the HAXPES peaks were defined with respect to the Fermi edge, and the spectral intensities were normalized to the total signal area.

The peak energy at 0.4 V shifted to a higher binding energy compared with that of the Pt foil and the line width also became broader due to the size effect of the NPs.[45,46] Upon increasing the voltage to 1.4 V, the Pt NPs were oxidized and a new $4f_{5/2}$ peak appeared at 77.55 eV, which is 3.1 eV higher than the main $4f_{5/2}$ peak for metallic Pt(0) at 74.45 eV. Correspondingly, the $4f_{7/2}$ peak was also seen at ~74.2 eV as a shoulder overlapped by the

metallic Pt(0) $4f_{5/2}$ peak (Figure 2(c)). In order to clarify the Pt oxidation state associated with the new peaks, we measured the Pt 4f spectra of the platinum(IV) oxide (PtO_2) powder. The Pt 4f peaks of PtO_2 showed a chemical shift of 3.7 eV from the Pt metal peaks. Moreover, the XPS Pt 4f spectra of a Pt–Co alloy catalyst in a deteriorated MEA after potential cycling between 0.6 V and 1.2 V showed clear peaks assigned to Pt(IV) at binding energies 4.4 eV higher than those of the Pt metal peaks.[47] Therefore, the *in situ* NAP-HAXPES suggests that the new oxidized peaks in the Pt 4f spectra at a voltage of 1.4 V originate from Pt(II) species. Pt(IV) does not exist on the Pt NPs at the Pt/C cathode in the MEA at normal operating voltages, because no peaks in the Pt(IV) energy region can be observed. This result is in good agreement with the *in situ* XAFS conclusion for the Pt NP catalysts in MEA Pt/C. [6,14-19] The *in situ* XAFS measurements demonstrated that the direct transformation from metallic Pt to mostly Pt(II) at the nanoparticle surfaces occurs at potentials above 1.2 V, exhibiting an isosbestic point in the XANES series, and no further oxidation to Pt(IV) was observed under fuel cell operating conditions.[6,14-19] The formation of crystalline α-PtO_2 and β-PtO_2 on Pt/C rotating disk electrodes after prolonged application of a large positive voltage has been reported previously, but such conditions are essentially different from the PEFC MEA Pt/C operating conditions.[48] Huang et al. reported two-dimensional (su)peroxo-like two-dimensional oxides and amorphous 3D α-PtO_2 are sequentially formed during the anodic polarization though in their work the applied potential was as more positive as 2.0 V.[49] Saveleva et al. proposed the different Pt oxidation mechanism at high anodic polarization by NAP-XPS study, consisting of adsorption of O/OH followed by nucleation of PtO/PtO_2 oxides and their subsequent three-dimensional growth.[10] In our case of the MEA Pt/C cathode electrocatalyst under H_2(anode)-4,000 Pa H_2O(cathode), the PtO_x exists as 2D species only on the outermost surface of the Pt nanoparticle from the result of the peak fit analysis for the NAP-HAXPES spectra at 1.4 V and the PtO_x species are situated as Pt^+ and Pt^{2+} as suggested by NAP-HAXPES as discussed later.

It was also reported that oxide growth first begins with the formation of a thin layer of PtO composition, on which PtO_2-composed oxide continues grows above ~1.2 V. However, for the case of thin oxide layers (1-2 layers), density functional theory calculations indicate the possibility of a stable phase of PtO composition with the (100) plane.[50] *Ex situ* electro-chemical (EC) XPS also identified Pt(II)-O and Pt(I)-OH at different Pt single crystal surfaces, but no Pt(IV)-oxygenate species were observed though it should be noted that the EC-XPS system was different from a PEFC MEA.[51]

It is noted that due to the vital importance of high proton mobility in the MEA, the oxygen reduction reaction in PEFCs occurs only under operating conditions with sufficient water, and the oxidation of Pt NP surfaces at the cathode also proceeds at the positive voltages under PEFC operating conditions. The present *in situ* NAP-HAXPES system allows us to observe the oxidation state of Pt NPs in the MEA Pt/C cathode layers as the apparatus can be operated at higher pressures than the saturated water vapor pressure at RT.

Although oxidized Pt 4f peaks were detected in Figure 2, the spectra are not of a sufficiently high quality for quantitative analysis and further discussion. Due to the limited beam time available at the synchrotron radiation facility, improving the S/N ratio of the spectra by simply performing the measurements over a longer time period is difficult. Instead, we exploited the fact that the photoionization cross sections of deep core levels in hard X-ray experiments are generally larger than those of the levels closer to the Fermi edge.[52] The signal intensity from the Pt 3d levels with a binding energy of around 2120 eV was about two orders of magnitude larger than that of the Pt 4f levels with a binding energy of approximately 78 eV, and hence the S/N ratio of the spectra was greatly improved and determination of the oxidation state of the Pt NP electrocatalysts from the Pt 3d levels was possible without the need for undesirable longer measurements.

Figure 3 shows the *in situ* Pt 3d HAXPES spectra of the samples, measured under the

same conditions as for the results shown in Figure 2. Comparison of Figures 2 and 3 shows that the spectral quality of the Pt 3d levels is noticeably improved relative to that of the Pt 4f levels, even for a measurement time of only 20 min per spectrum, due to the much higher hard X-ray cross sections of the Pt 3d region. The spectrum at 0.4 V was broader than that of Pt foil, and a definite shoulder peak at 1.4 V was observed on the higher energy side of the spectrum (Figure 3(c)). Broader peaks due to the shorter life time of deep core-hole levels prevented high resolution observation of these contributions due to their small differences in binding energies. For quantitative compositional analysis, the Pt 3d spectra were decomposed into three components: Pt1, Pt2, and Pt3. Considering the Pt 4f spectra in Figure 2, we straightforwardly assigned the Pt1 component at 2122.0 eV to metallic Pt(0), and Pt3 at 2125.1 eV to Pt(II). The Pt2 component at 2123.3 eV that occurs at an energy intermediate between the binding energies for Pt(0) and Pt(II) can be assigned to Pt(I) species such as Pt-OH, but may also contain contributions from electronically modified Pt species such as Pt atoms at the edge and corner sites in the Pt NPs. Since the Pt2 intensity in Figure 3 was larger at 1.4 V than at 0.4 V, the Pt-OH oxidized species should be considered a major species in Pt2 at 1.4 V. Edge/corner Pt atoms may also exist because the adsorption of hydroxyl groups on Pt NPs is not expected to occur at 0.4 V. In the curve-fitting analysis, the Doniach–Sunjic function with a small asymmetric parameter was used for the metallic component (Pt1) and symmetric Gaussian functions were used for the other components (Pt2 and Pt3). It was confirmed by deconvolution that the *in situ* NAP-HAXPES spectrum at 0.4 V comprises two (Pt1 and Pt2) components, and the spectrum at 1.4 V also contains the Pt3 component in addition to the Pt1 and Pt2 components. Hence, analysis of the *in situ* NAP-HAXPES spectra provides quantitative information about the oxidization/reduction of the Pt NPs in MEA Pt/C cathode catalysts.

The measurement time for the Pt 3d spectra is much shorter than that for the Pt 4f spectra because of the two orders of magnitude more intense signals originating from the 3d levels.

This favorable feature is quite useful for the investigation of voltage-dependent Pt oxidation states because it is necessary to obtain many spectra in a limited beam time. On the contrary, the Pt 3d peaks become broader than the Pt 4f peaks due to the much shorter lifetime of the core-hole states of the Pt 3d levels, resulting in a somewhat small energy separation between the peaks. When higher energy resolution is required, observation of the Pt 4f levels with a longer measurement time may be more suitable.

The voltage dependence of the oxidation state of the Pt atoms in MEA Pt NPs was observed by measuring the *in situ* Pt 3d NAP-HAXPES spectra in the 0.2-1.4 V range, either increasing or decreasing the voltage in steps of 0.2 V, as shown in Figures 4(a) and (b), respectively. The Shirley background was subtracted from these spectra and, subsequently, the spectra were normalized by their respective total areas. Inspection of Figure 4(a) shows similar spectral shapes from 0.2 V to 0.8 V. A shoulder peak corresponding to the oxidized state appeared at 1.0 V and grew until 1.4 V. Upon decreasing the voltage (Figure 4(b)), the intensity of the shoulder peak at 1.4 V did not decrease at 1.2 V at all, and the shoulder intensity did not decrease significantly until 1.0 V. The spectrum began to change below 1.0 V and the shoulder peak disappeared completely at 0.6 V. The spectra were deconvoluted to three components similar to the analysis shown in Figure 3. The component fractions for Pt1, Pt2 and Pt3 are plotted in Figures 4(c), (d), and (e), respectively. The chemical state of Pt exhibited a distinct hysteresis while increasing and decreasing the voltage. A similar hysteresis has also been reported in the transformations of the Pt valence and the coordination numbers of Pt-Pt and Pt-O bonds by *in situ* XAFS analysis, where the three different oxidation states of Pt NPs in MEA were not quantitatively discriminated.[6,14-19]

We also examined the voltage dependence of the oxidation states of Pt NPs in Pt/C with a larger average particle size of 4.8 nm (TEC10E50E-HT). The Pt 4f peak was broader than that of Pt foil, and the peak was shifted to the high-binding-energy side, although the variations

were smaller compared with the case of Pt NPs with a smaller diameter of 2.6 nm (TEC10E50E). A similar tendency was also observed for the Pt $3d_{5/2}$ peak. The result reflects a particle size effect on the Pt electronic state.[45,53]

Figures 5(a) and (b) show the spectra for Pt/C (TEC10E50E-HT) while increasing and decreasing the voltage, respectively, in a similar manner to that for Pt/C(TEC10E50E) presented in Figure 4. The oxidation peak at around 2125 eV appeared or disappeared depending on the voltage. The spectra were also deconvoluted into Pt1, Pt2, and Pt3 components with binding energies of 2122.0 eV, 2123.3 eV, and 2125.1 eV, respectively. Figures 5(c)-(e) show similar hysteresis features for each Pt peak, although the concentration variations are less pronounced.

We now discuss the structural transformations of the Pt NPs based on the quantitative analyses of the *in situ* NAP-HAXPES results. Assuming an fcc cubo-octahedral structure of Pt NPs, average cubo-octahedral Pt NPs with diameters of 2.6 nm (TEC10E50E) and 4.8 nm (TEC10E50E-HT) comprise 586 and 4033 Pt atoms, respectively. In these NPs, the ratios of inner to outer Pt atoms are 54% for 586 atoms and 73% for 4033 atoms. These values agree well with the concentrations of the metal component Pt1 in Figures 4(c) and 5(c) at the voltage of 1.4 V, at which the Pt NPs are highly oxidized. These results suggest that only the surface Pt atoms in the Pt NPs of the MEAs are oxidized, and the atoms in the NP core maintain their metallic state, as illustrated in Figure 6.

Previous *in situ* XAFS measurements for similar samples also indicated that the oxygen atoms were located both on the outermost surfaces and in the subsurface of Pt NPs at 1.4 V.[15,18] These findings by different techniques were compatible with each other, but more detailed information can be derived from the present results obtained by *in situ* NAP-HAXPES, which form the basis of the following discussion. When the Pt(111) single-crystal surface is oxidized, the resultant surface oxide is known to exhibit substantial buckling of both O and Pt atoms.[30,54]

The upward-buckled Pt atoms are chemically bonded to both surface-chemisorbed and subsurface oxygen atoms, whereas the downward-buckled Pt atoms are bonded to surface hydroxyls or subsurface oxygen atoms. In this configuration, only the buckled Pt atoms on the surface change their valence, and the oxidation may not significantly influence the second layer of Pt atoms. The upward-buckled and downward-buckled Pt atoms at voltages >1.0 V could be ascribed to Pt(II) and Pt(I), respectively.

When oxygen gas at a partial pressure of 1,000 Pa was supplied with the water vapor to the cathode, no peak related to the oxidation of Pt was detected in the Pt 3d spectra at voltages <0.8 V because of the low oxygen partial pressure. To detect the oxidation state under oxygen gas flow we may need to operate the measurement cell at an appropriate oxygen partial pressure.

Measuring the electronic state in the valence band is important because the valence band, especially the states near the Fermi edge, reflects the catalytic activity of the material. Meanwhile, the cross section of the valence band is very low when hard X-rays with an 8 keV photon energy are used as the excitation source. It takes approximately two hours to obtain the valence band spectra of the Pt NPs in the PEFC electrode at a sufficient quality using the present HAXPES system. Figure 7 shows the valence band spectra for Pt/C (TEC10E50E) and Pt/C (TEC10E50E-HT) at 0.4 V and 1.4 V, together with that for the Pt foil for comparison, which exhibits a sharp peak that appears near the Fermi edge. The peak intensity decreases in the order of foil, TEC10E50E-HT, TEC10E50E, indicating that the catalytic activity increases as the particle size decreases.[55] The voltage dependence of the valence band of the Pt NPs was also observed under the same conditions as in Figures 2 and 3. In the spectra of TEC10E50E (Fig. 7(c)), the spectral shapes at 0.4 V and 1.4 V are completely different from each other. The densities of the electronic states near the Fermi edge and around 4.5 eV decreased at 1.4 V, whereas those around 3 eV increased compared with that at 0.4 V, resulting in a simple valence band structure for TEC10E50E at 1.4 V. According to the results shown in Figure 4(e), the

oxidized Pt atoms comprised about 25% of the Pt NPs at 1.4 V. Therefore, features of the valence band of PtO [56] appear in the spectra at 1.4 V. The difference between the valence bands of TEC10E50E-HT at 0.4 V and 1.4 V was small, because the fraction of oxidized Pt(II) in the NPs was only about 10% according to Figure 5(e).

4 Conclusions

In the present work, we have improved the performance of our *in situ* NAP-HAXPES measurement system, and investigated in detail the oxidation states of Pt NP electrocatalysts in the cathode layer of PEFCs by applying a voltage between the electrodes. The optimum water vapor pressure for making *in situ* NAP-HAXPES measurements was approximately 4,000 Pa. Under this pressure, the MEA retains sufficient moisture to transport protons and the liquid water layer over the Pt NPs was thin enough to transmit photoelectrons from the Pt NPs. Under the optimum vapor pressure, the specific voltage-dependent changes of the Pt 3d and Pt 4f HAXPES spectral shapes originating from oxidation/reduction of the Pt atoms were successfully detected. The oxidized Pt appearing at voltages >1.0 V was unambiguously ascribed not to tetravalent Pt but to divalent Pt. In the Pt 3d spectra, the Pt component ratio as a function of voltage showed definite hysteresis for each Pt species. Quantitative analysis of the peak fitting for NPs with different particle sizes indicated that the Pt oxidization only occurred at the surface of the Pt NPs, and no inner Pt atoms were involved in the electro-oxidation. In the valence band spectra, the density of electronic states near the Fermi edge reduced with decreasing particle size, indicating higher activities for smaller Pt nanoparticles. A change in the valence band structure due to oxidation of the Pt atoms was also observed at large positive voltages.

This oxidative reaction takes place at the MEA with sufficient water to facilitate high proton mobility from the anode to the cathode through the Nafion electrolyte membrane. *In situ* NAP-HAXPES is a useful method for the observation of the electronic states of wet

samples at high water vapor pressures, which allows us to perform *in situ* hard X-ray photoelectron spectroscopic investigations of active Pt NPs in Pt/C cathode layers under PEFC operating conditions.

Acknowledgments

These experiments were performed with the approval of SPring-8 (Nos. 2014A7810, 2014A7811, 2014B7810, 2014B7811, 2015A7810 and 2015B7810). This work was supported by the Polymer Electrolyte Fuel Cell Program from the New Energy and Industrial Technology Development Organization (NEDO) and by the Grants-in-Aid for Scientific Research (KAKENHI) Grant Number 15H05489 from the Japan Society for the Promotion of Science.

References

1. R. Borup, J. Meyers, B. Pivovar, Y. S. Kim, R. Mukundan, N. Garland, D. Myers, M. Wilson, F. Garzon, D. Wood, P. Zelenay, K. More, K. Stroh, T. Zawodzinski, J. Boncella, J. E. McGrath, M. Inaba, K. Miyatake, M. Hori, K. Ota, Z. Ogumi, S. Miyata, A. Nishikata, Z. Siroma, Y. Uchimoto, K. Yasuda, K. Kimijima and N. Iwashita, Chemical reviews, 2007, **107**, 3904–39051.

2. M. K. Debe, Nature, 2012, **486**, 43–51.

3. A. Rabis, P. Rodriguez and T. J. Schmidt, ACS Catalysis, 2012, **2**, 864–890.

4. K. Nagasawa, S. Takao, S. Nagamatsu, G. Samjeské, O. Sekizawa, T. Kaneko, K. Higashi, T. Yamamoto, T. Uruga and Y. Iwasawa, Journal of the American Chemical Society, 2015, **137**, 12856-12864.

5. K. Kunimatsu, T. Yoda, D. A. Tryk, H. Uchida, and M.Watanabe, Phys. Chem. Chem. Phys., 2010, **12**, 621-629.

6. M. Tada, S. Murata, T. Asakoka, K. Hiroshima, K. Okumura, H. Tanida, T. Uruga, H. Nakanishi, S. Matsumoto, Y. Inada, M. Nomura, and Y. Iwasawa, Angewandte Chemie International Edition, 2007, **46**, 4310-4315.

7. N. Ishiguro, T. Saida, T. Uruga, S. Nagamatsu, O. Sekizawa, K. Nitta, T. Yamamoto, S. Ohkoshi, Y. Iwasawa, T. Yokoyama, and M. Tada, ACS Catalysis, 2012, **2**, 1319-1330.

8. H. S. Casalongue, S. Kaya, V. Viswanathan, D. J. Miller, D. Friebel, H. A. Hansen, J. K. Nørskov, A. Nilsson, and H. Ogasawara, Nature Communications, 2013, **4**, 2817.

9. R. Arrigo, M. Hävecker, M. E. Schuster, C. Ranjan, E. Stotz, A. Knop-Gericke, and R. Schlögl, Angewandte Chemie International Edition, 2013, **52**, 11660-11664.

10. V. A. Saveleva, V. Papaefthimiou, M. K. Daletou, W. H. Doh, C. Ulhaq-Bouillet, M. Diebold, S. Zafeiratos, and E. R. Savinova, The Journal of Physical Chemistry C, 2016, **120**, 15930-15940.

11. H. Niwa, H. Kiuchi, J. Miyawaki, Y. Harada, M. Oshima, Y. Nabae, and T. Aoki, Electrochemistry Communications, 2013, **35**, 57-60.

12. H. Yoshida, H. Omote, and S. Takeda, Nanoscale, 2014, **6**, 13113-13118.

13. H. L. Xin, S. Alayoglu, R. Tao, A. Genc, C.-M. Wang, L. Kovarik, E. A. Stach, L.-W.Wang, M. Salmeron, G. a. Somorjai, and H. Zheng, Nano letters, 2014, **14**, 3203-3207.

14. S. Takao, O. Sekizawa, G. Samjeské, S. Nagamatsu, T. Kaneko, T. Yamamoto, K. Higashi, K. Nagasawa, T. Uruga, and Y. Iwasawa, *J. Phys. Chem. Lett.,*2015, **6**, 2121–2126 .

15. S. Nagamatsu, T. Arai, M. Yamamoto, T. Ohkura, H. Oyanagi, T. Ishizaka, H. Kawanami, T. Uruga, M. Tada, and Y. Iwasawa, The Journal of Physical Chemistry C, 2013, **117**, 13094-13107.

16. K. Nagasawa, S. Takao, K. Higashi, S. Nagamatsu, G. Samjeske, Y. Imaizumi, O. Sekizawa, T. Yamamoto, T. Uruga, and Y. Iwasawa, Physical Chemistry Chemical Physics, 2014, **16**, 10075.

17. M. Tada, T. Uruga, and Y. Iwasawa, Catalysis Letters 2015, **145**, 58-70.

18. S. Nagamatsu, S. Takao, G. Samjeské, K. Nagasawa, O. Sekizawa, T. Kaneko, K. Higashi, T. Uruga, S. Gayen, S. Velaga, M. K. Saniyal, and Y. Iwasawa, Surface Science, 2016, **648**, 100-113.

19. T. Kaneko, G. Samjeské, S. Nagamatsu, K. Higashi, O. Sekizawa, S. Takao, T. Yamamoto, X. Zhao, T. Sakata, T. Uruga, and Y. Iwasawa, *J. Phys. Chem. C*, 2016, **120**, 24250–24264.

20. H. Siegbahn and K. Siegbahn, Journal of Electron Spectroscopy and Related Phenomena, 1973, **2**, 319-325.

21. E. M. Vass, M. Hävecker, S. Zafeiratos, D. Teschner, A. Knop-Gericke, and R. Schlögl, Journal of Physics: Condensed Matter, 2008, **20**, 184016.

22. M. Salmeron and R. Schlögl, Surface Science Reports, 2008, **63**, 169-199.

23. D. Frank Ogletree, H. Bluhm, E. D. Hebenstreit, and M. Salmeron, Nuclear Instruments and Methods in Physics Research Section A: Accelerators, Spectrometers, Detectors and Associated Equipment, 2009, **601**, 151-160.

24. H. Bluhm, Journal of Electron Spectroscopy and Related Phenomena, 2010, **177**, 71-84.

25. D. E. Starr, Z. Liu, M. Hävecker, A. Knop-Gericke, and H. Bluhm, Chemical Society reviews, 2013, **42**, 5833-5857.

26. M. A. Brown, A. B. Redondo, I. Jordan, N. Duyckaerts, M.-T. Lee, M. Ammann, F. Nolting, A. Kleibert, T. Huthwelker, J.-P. Machler, M. Birrer, J. Honegger, R.Wetter, H. J.Worner, and J. A. van Bokhoven, The Review of scientific instruments, 2013, **84**, 073904.

27. X. Liu, W. Yang, and Z. Liu, Advanced materials, 2014, **26**, 7710-7729.

28. E. J. Crumlin, Z. Liu, H. Bluhm,W. Yang, J. Guo, and Z. Hussain, Journal of Electron Spectroscopy and Related Phenomena, 2015, **200**, 264-273.

29. F. Tao, M. E. Grass, Y. Zhang, D. R. Butcher, J. R. Renzas, Z. Liu, J. Y. Chung, B. S. Mun, M. Salmeron, and G. A. Somorjai, Science, 2008, **322**, 932-934.

30. D. J. Miller, H. Öberg, S. Kaya, H. S. Casalongue, D. Friebel, T. Anniyev, H. Ogasawara, H. Bluhm, L. G. M. Pettersson, and A. Nilsson, Physical Review Letters, 2011, **107**, 195502.

31. D. Miller, H. Sanchez Casalongue, H. Bluhm, H. Ogasawara, A. Nilsson, and S. Kaya, Journal of the American Chemical Society, 2014, **136**, 6340-6347.

32. S. Nemšák, A. Shavorskiy, O. Karslioglu, I. Zegkinoglou, A. Rattanachata, C. S. Conlon, A. Keqi, P. K. Greene, E. C. Burks, F. Salmassi, E. M. Gullikson, S.-H. Yang, K. Liu, H. Bluhm, and C. S. Fadley, Nature Communications, 2014, **5**, 5441.

33. Y. Takagi, H. Wang, Y. Uemura, E. Ikenaga, O. Sekizawa, T. Uruga, H. Ohashi, Y. Senba, H. Yumoto, H. Yamazaki, S. Goto, M. Tada, Y. Iwasawa, and T. Yokoyama, Applied Physics Letters, 2014, **105**, 131602.

34. O. Karslıoğlu, S. Nemšák, I. Zegkinoglou, A. Shavorskiy, M. Hartl, F. Salmassi, E. Gullikson, M.-L. Ng, C. Rameshan, B. Rude, D. Bianculli, A. Cordones-Hahn, S. Axnanda, E. Crumlin, P. N. Ross, C. M. Schneider, Z. Hussain, Z. Liu, C. S. Fadley, and H. Bluhm, Faraday Discuss, 2015, **180**, 35-53.

35. S. Axnanda, E. J. Crumlin, B. Mao, S. Rani, R. Chang, P. G. Karlsson, M. O. M. Edwards, M. Lundqvist, R. Moberg, P. Ross, Z. Hussain, and Z. Liu, Scientific Reports, 2015, **5**, 9788.

36. O. Sekizawa, T. Uruga, M. Tada, K. Nitta, K. Kato, H. Tanida, K. Takeshita, S. Takahashi, M. Sano, H. Aoyagi, A. Watanabe, N. Nariyama, H. Ohashi, H. Yumoto, T. Koyama, Y. Senba, T. Takeuchi, Y. Furukawa, T. Ohata, T. Matsushita, Y. Ishizawa, T.

Kudo, H. Kimura, H. Yamazaki, T. Tanaka, T. Bizen, T. Seike, S. Goto, H. Ohno, M. Takata, H. Kitamura, T. Ishikawa, T. Yokoyama, and Y. Iwasawa, Journal of Physics: Conference Series, 2013, **430**, 012020.

37. O. Sekizawa, T. Uruga, Y. Takagi, K. Nitta, K. Kato, H. Tanida, K. Uesugi, M. Hoshino, E. Ikenaga, K. Takeshita, S. Takahashi, M. Sano, H. Aoyagi, A. Watanabe, N. Nariyama, H. Ohashi, H. Yumoto, T. Koyama, Y. Senba, T. Takeuchi, Y. Furukawa, T. Ohata, T. Matsushita, Y. Ishizawa, T. Kudo, H. Kimura, H. Yamazaki, T. Tanaka, T. Bizen, T. Seike, S. Goto, H. Ohno, M. Takata, H. Kitamura, T. Ishikawa, M. Tada, T. Yokoyama, and Y. Iwasawa, Journal of Physics: Conference Series, 2016, **712**, 012142.

38. S. K. Eriksson, M. Hahlin, J. M. Kahk, I. J. Villar-Garcia, M. J. Webb, H. Grennberg, R. Yakimova, H. Rensmo, K. Edström, A. Hagfeldt, H. Siegbahn, M. O. M. Edwards, P. G. Karlsson, K. Backlund, J. Åhlund, D. J. Payne, The Review of scientific instruments, 2014, **85**, 075119.

39. N. Ishiguro, S. Kityakarn, O. Sekizawa, T. Uruga, T. Sasabe, K. Nagasawa, T. Yokoyama, and M. Tada, The Journal of Physical Chemistry C, 2014, **118**, 15874-15883.

40. K. Oka, Y. Ogura, and Y. Izumi, Journal of Power Sources, 2014, **258**, 83-88.

41. Y. Hashimasa and T. Numata, International Journal of Hydrogen Energy, 2015, **40**, 11543-11549.

42. D. F. Ogletree, H. Bluhm, G. Lebedev, C. S. Fadley, Z. Hussain, and M. Salmeron, Review of Scientific Instruments, 2002, **73**, 3872-3877.

43. A. Muñoz, J. C. Oller, F. Blanco, J. D. Gorfinkiel, P. Limão-Vieira, and G. García, Physical Review A, 2007, **76**, 052707.

44. D. Emfietzoglou and H. Nikjoo, Radiation research **167**, 110-120.

45. M. G. Mason, Physical Review B, 1983, **27**, 748-762.

46. W. Eberhardt, P. Fayet, D. M. Cox, Z. Fu, A. Kaldor, R. Sherwood, and D. Sondericker, Physical Review Letters, 1990, **64**, 780-783.

47. S. Hidai, M. Kobayashi, H. Niwa, Y. Harada, M. Oshima, Y. Nakamori, and T. Aoki, Journal of Power Sources, 2012, **215**, 233-239.

48. H. Imai, K. Izumi, M. Matsumoto, Y. Kubo, K. Kato and Y. Imai, Journal of the American Chemical Society, 2009, **131**, 6293-6300.

49. Y.-F. Huang, P. J. Kooyman, and M. T. M. Koper, Nature Communications, 2016, **7** 12440.

50. T. Jacob, Journal of Electroanalytical Chemistry, 2007, **607**, 158-166.

51. M. Wakisaka, Y. Udagawa, H. Suzuki, H. Uchida and M. Watanabe, Energy & Environmental Science, 2011, **4**, 1662-1666.

52. J. Yeh and I. Lindau, Atomic Data and Nuclear Data Tables, 1985, **32**, 1-155.

53. T. Cheung, Surface Science, 1984, **140**, 151-164.

54. J. M. Hawkins, J. F. Weaver, and A. Asthagiri, Physical Review B, 2009, **79**, 125434.

55. M. Nesselberger, M. Roefzaad, R. F. Hamou, P. U. Biedermann, F. F. Schweinberger, S. Kunz, K. Schloegl, G. K. H. Wiberg, S. Ashton, U. Heiz, K. J. J. Mayrhofer, and M. Arenz, Nature materials, 2013, **12**, 919-924.

56. K. C. Hass and A. E. Carlsson, Physical Review B, 1992, **46**, 4246-4249.

Figure captions:

FIG. 1. (a) Cyclic voltammograms and (b) Pt $3d_{5/2}$ spectra recorded with different water vapor pressures at the cathode. The scan rate used for the cyclic voltammetry measurements was 20 mV/s. The Pt $3d_{5/2}$ spectra were recorded a voltage corresponding to the open-circuit voltage (0.12 V). TEC10E50E was used as the catalyst in the electrode. (c) Water pressure dependence of the reduction peak intensity at around 0.75 V in the cyclic voltammograms (red) and the Pt $3d_{5/2}$ peak intensity (blue). The dashed lines are solely for guiding the eye.

FIG. 2. Pt 4f spectra of Pt foil and the Pt/C catalyst at the cathode ($h\nu$ = 7.94 keV). The Pt foil spectrum was recorded under high vacuum, and the other spectra were recorded under a water pressure of 4,000 Pa at the cathode.

FIG. 3. Pt $3d_{5/2}$ spectra of Pt foil and the Pt/C catalyst at the cathode ($h\nu$ = 7.94 keV). The Pt foil spectrum was recorded under high vacuum and the other spectra were recorded under a water pressure of 4,000 Pa at the cathode. The black dots correspond to the experimental results and the solid red lines to the fitted curves with three components of Pt1, Pt2, and Pt3.

FIG. 4. (a,b) *In situ* NAP-HAXPES Pt $3d_{5/2}$ spectra of the Pt/C catalyst with an average diameter of 2.6 nm (TEC10E50E) at the cathode for various cell voltages. The voltage is (a) increasing or (b) decreasing. (c–e) Bias voltage dependence of the concentration of the Pt chemical states (c) Pt1, (d) Pt2, and (e) Pt3 (see the text and figure 3 for descriptions of the components) obtained by curve fitting.

FIG. 5. (a,b) *In situ* NAP-HAXPES Pt $3d_{5/2}$ spectra of the Pt/C catalyst with an average diameter of 4.8 nm (TEC10E50E-HT) at the cathode for various cell voltages. The voltage is (a) increasing or (b) decreasing. (c–e) Bias voltage dependence of the concentration of Pt chemical states (c) Pt1, (d) Pt2, and (e) Pt3 obtained by curve fitting.

FIG. 6. Schematic showing the voltage dependent transformation of Pt NPs. (a) An NP of TEC10E50E with a diameter of 2.6 nm corresponds to the fcc cubo-octahedral-structured NP with four edge atoms (N_{edge}). The total number of atoms (N_{total}) in the NP is 586, and the number of the surface atoms ($N_{surface}$) is 272. (b) An NP of TEC10E50E-HT with a diameter of 4.8 nm corresponds to the fcc cubo-octahedral-structured NPs with N_{edge} = 7 atoms, N_{total} = 4033 atoms, and $N_{surface}$ = 1082 atoms. The dispersions (D = $N_{surface}$ / N_{total}) of the NPs with N_{edge} = 4 or 7 atoms are 0.46 and 0.27, respectively. These values agree well with the ratio of atoms with non-zero valence in the NPs at 1.4 V from the XPS measurements of the Pt $3d_{5/2}$ peak (Pt2+Pt3), indicating that only the surface atoms change their valence.

FIG. 7. Valence band spectra of Pt foil and the Pt/C catalysts with average diameters of 2.6 nm (TEC10E50E) and 4.8 nm (TEC10E50E-HT) at the cathode ($h\nu$ = 7.94 keV). The Pt foil spectrum was recorded under high vacuum and the other spectra were recorded under a water pressure of 4,000 Pa at the cathode. The black and red lines correspond to the spectra recorded at 0.4 and 1.4 V, respectively.

FIG. 1.

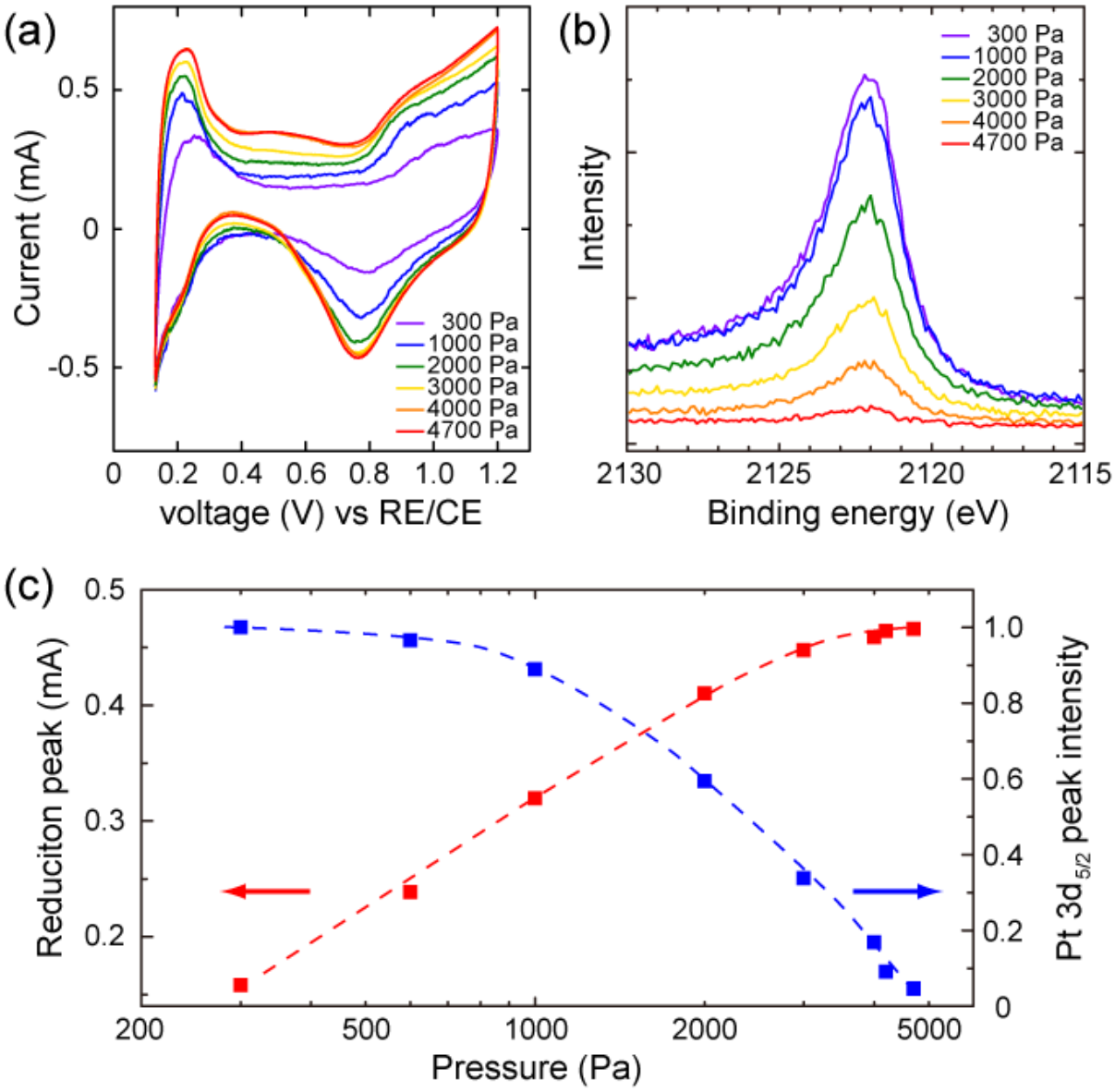
(a)
Current (mA)
0.5
0
-0.5
0
0.2
0.4
0.6
0.8
1.0
1.2
voltage (V) vs RE/CE
300 Pa
1000 Pa
2000 Pa
3000 Pa
4000 Pa
4700 Pa
(b)
Intensity
2130
2125
2120
2115
Binding energy (eV)
(c)
Reduciton peak (mA)
0.5
0.4
0.3
0.2
200
500
1000
2000
5000
Pressure (Pa)
1.0
0.8
0.6
0.4
0.2
0
Pt 3d5/2 peak intensity

FIG. 2.

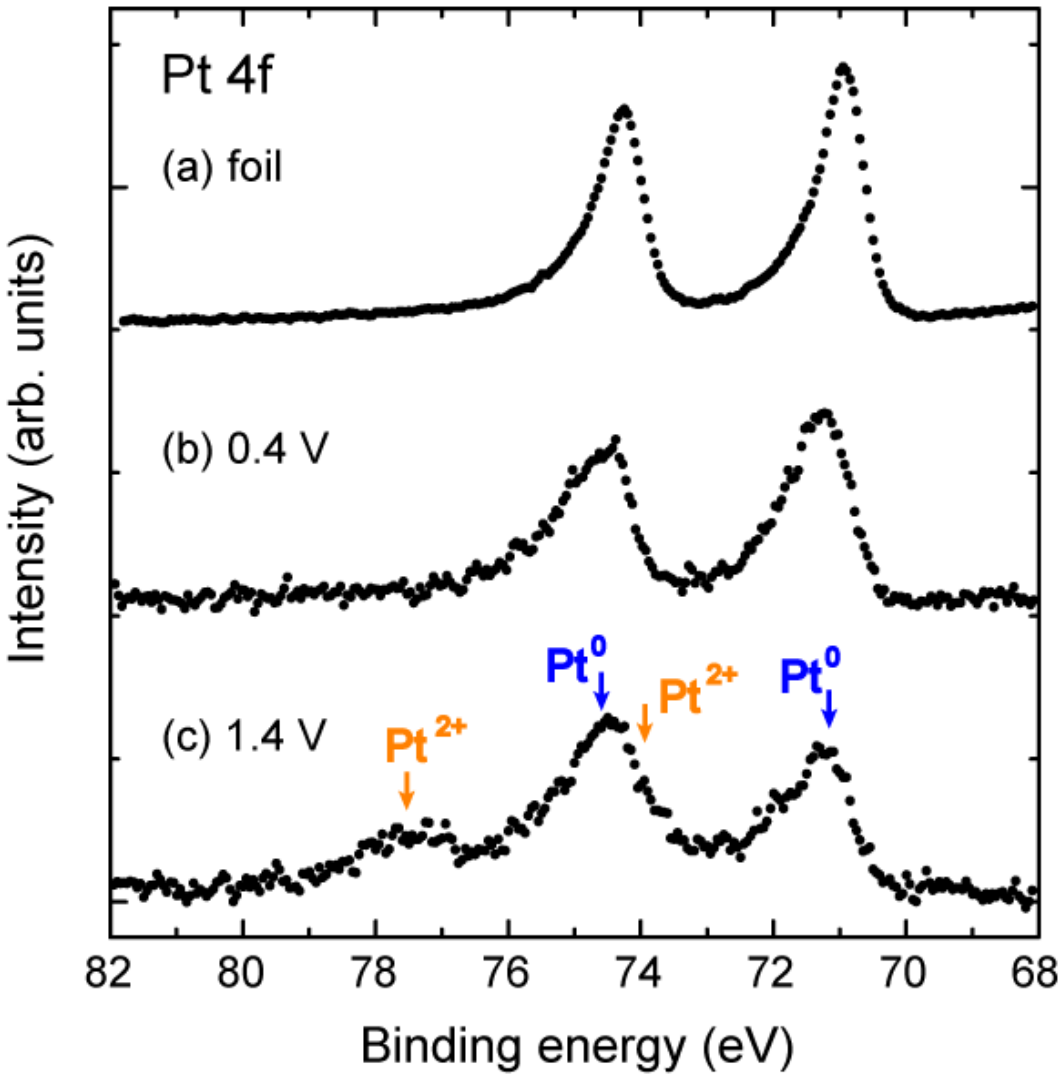
Pt 4f
(a) foil
(b) 0.4 V
(c) 1.4 V
Pt0
Pt2+
Pt2+
Pt0
Intensity (arb. units)
82
80
78
76
74
72
70
68
Binding energy (eV)

FIG. 3.

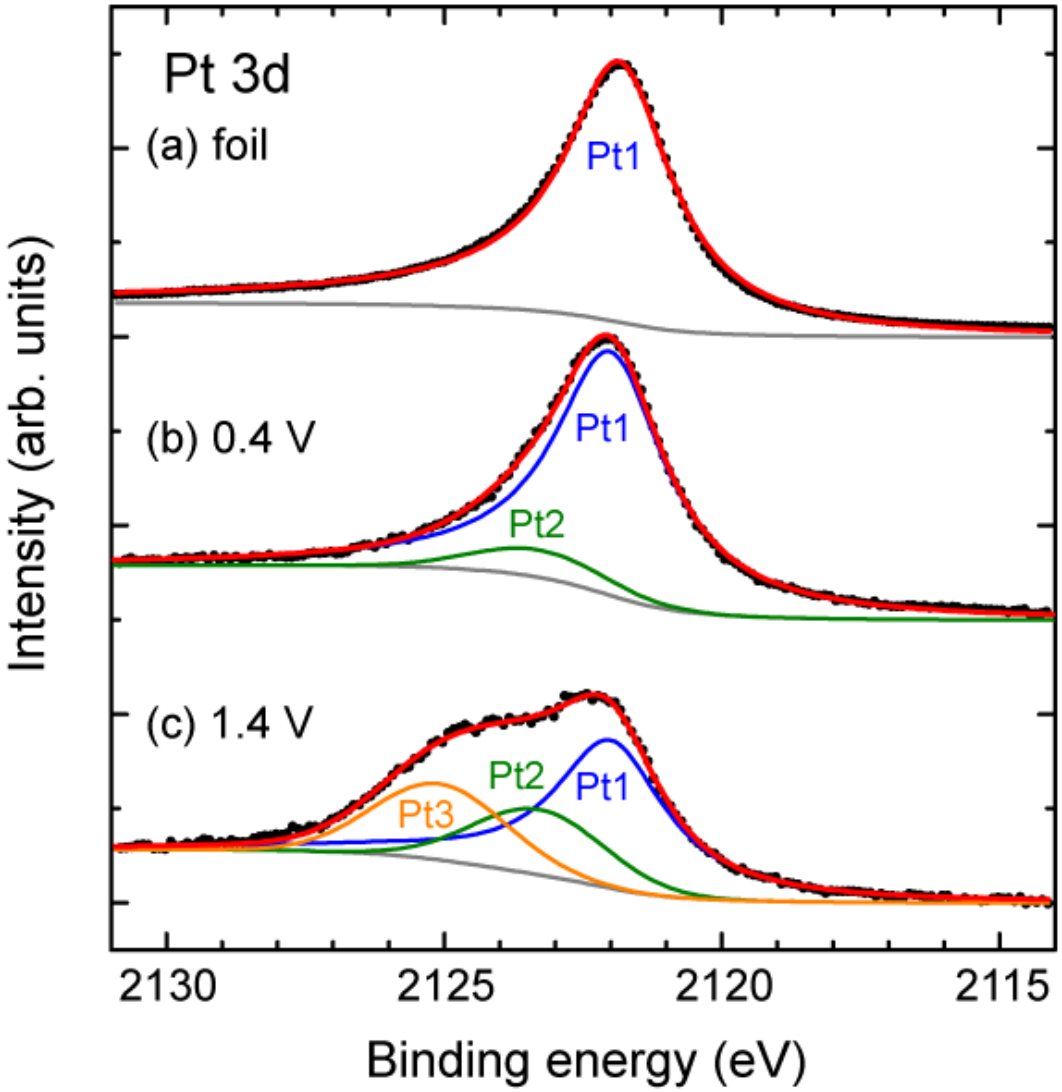
Pt 3d
(a) foil
Pt1
(b) 0.4 V
Pt1
Pt2
(c) 1.4 V
Pt2
Pt1
Pt3
Intensity (arb. units)
2130
2125
2120
2115
Binding energy (eV)

FIG. 4

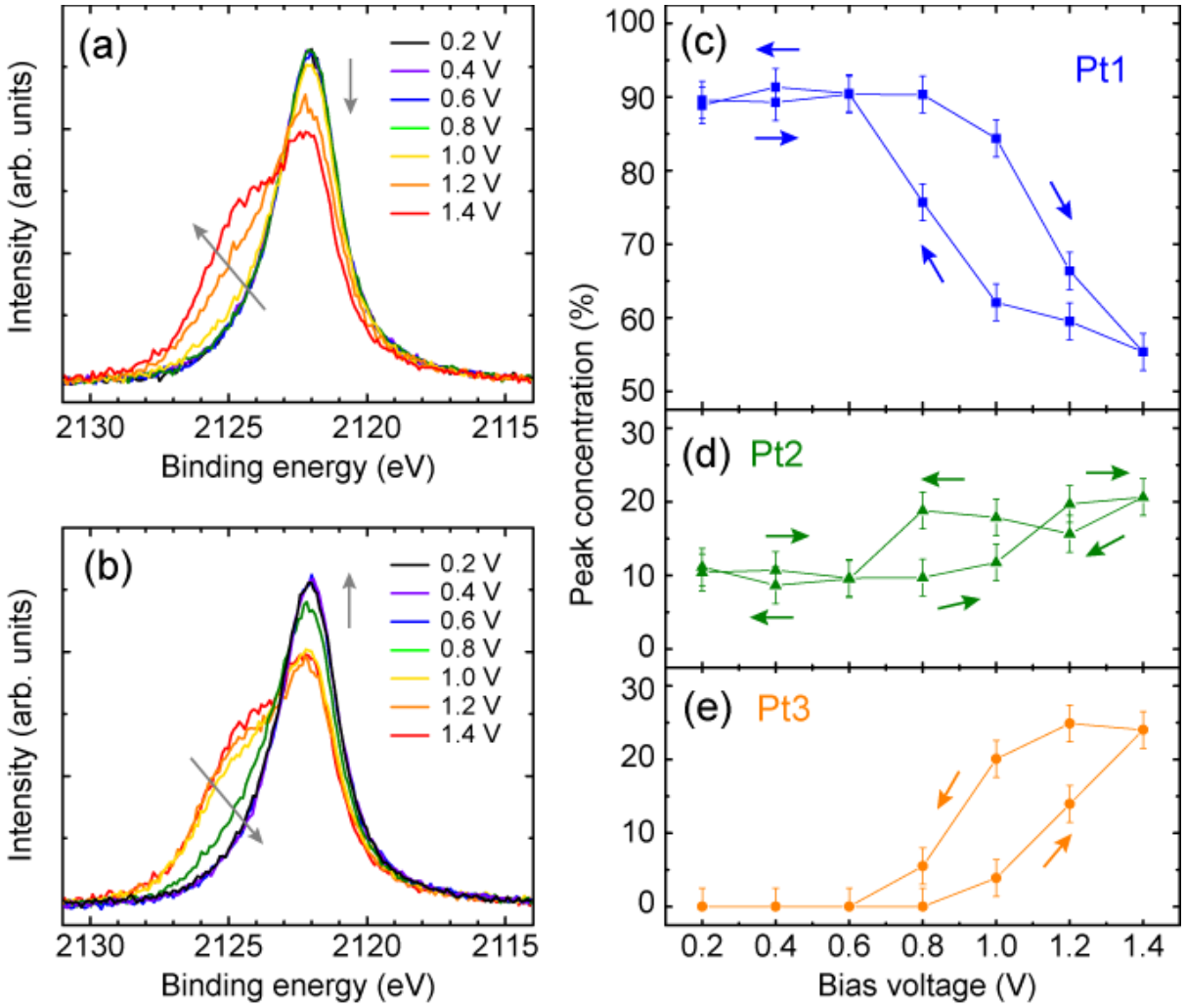
(a)
0.2 V
0.4 V
0.6 V
0.8 V
1.0 V
1.2 V
1.4 V
Intensity (arb. units)
2130
2125
2120
2115
Binding energy (eV)
(b)
0.2 V
0.4 V
0.6 V
0.8 V
1.0 V
1.2 V
1.4 V
Intensity (arb. units)
2130
2125
2120
2115
Binding energy (eV)
(c)
Pt1
(d)
Pt2
(e)
Pt3
Peak concentration (%)
100
90
80
70
60
50
30
20
10
0
30
20
10
0
0.2
0.4
0.6
0.8
1.0
1.2
1.4
Bias voltage (V)

FIG. 5.

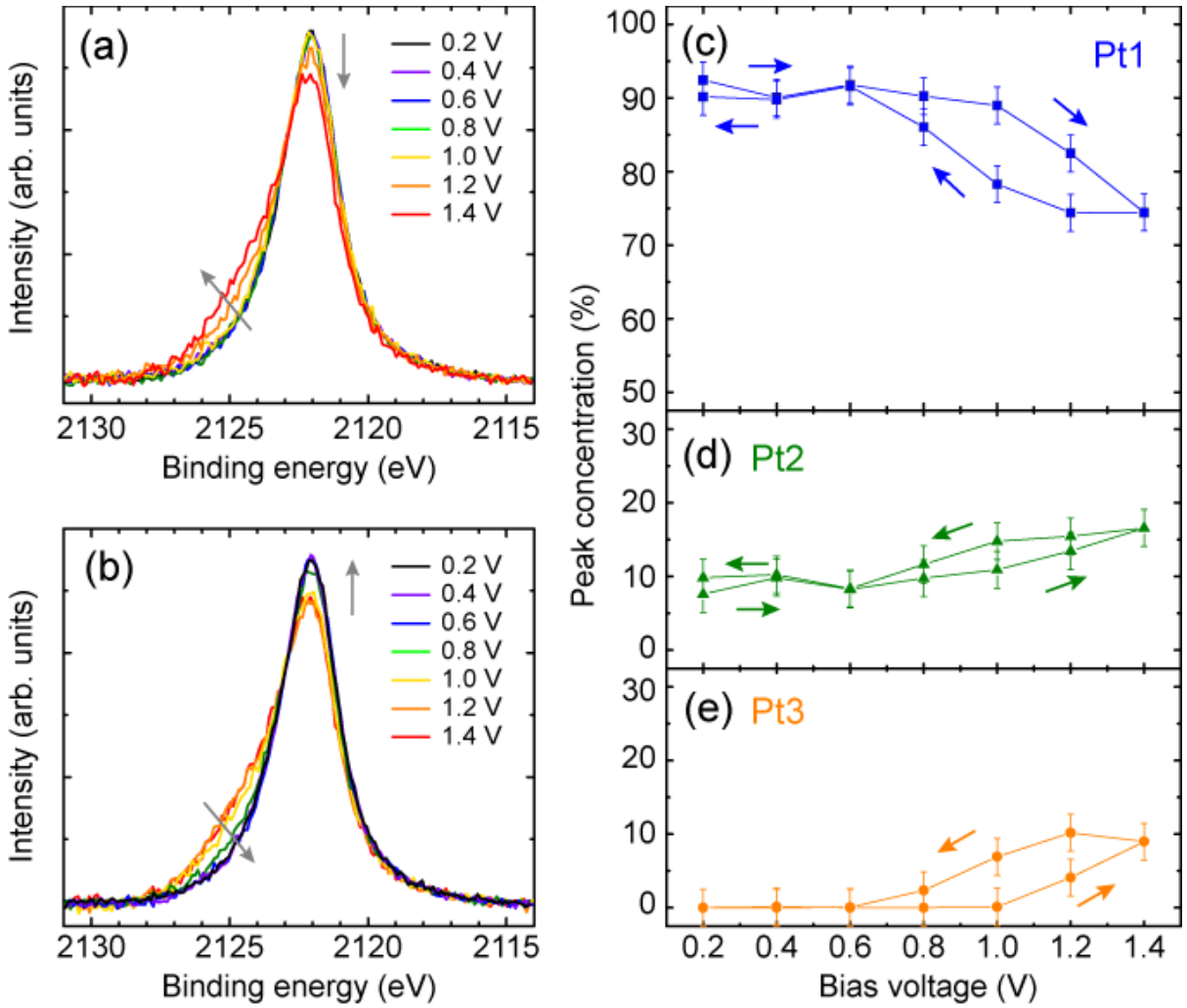
(a)
0.2 V
0.4 V
0.6 V
0.8 V
1.0 V
1.2 V
1.4 V
Intensity (arb. units)
2130
2125
2120
2115
Binding energy (eV)
(b)
0.2 V
0.4 V
0.6 V
0.8 V
1.0 V
1.2 V
1.4 V
Intensity (arb. units)
2130
2125
2120
2115
Binding energy (eV)
(c)
Pt1
(d)
Pt2
(e)
Pt3
Peak concentration (%)
100
90
80
70
60
50
30
20
10
0
30
20
10
0
0.2
0.4
0.6
0.8
1.0
1.2
1.4
Bias voltage (V)

FIG. 6

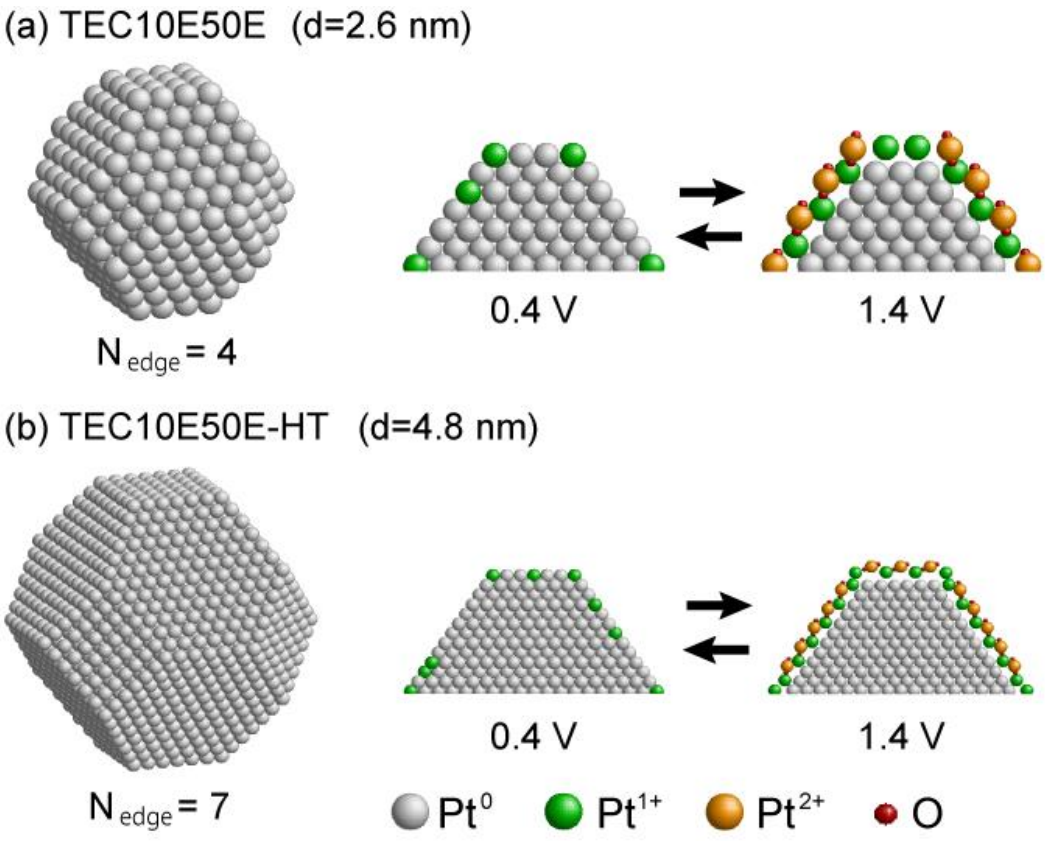
(a) TEC10E50E (d=2.6 nm)
N edge = 4
0.4 V
1.4 V
(b) TEC10E50E-HT (d=4.8 nm)
N edge = 7
0.4 V
1.4 V
Pt0
Pt1+
Pt2+
O

FIG. 7

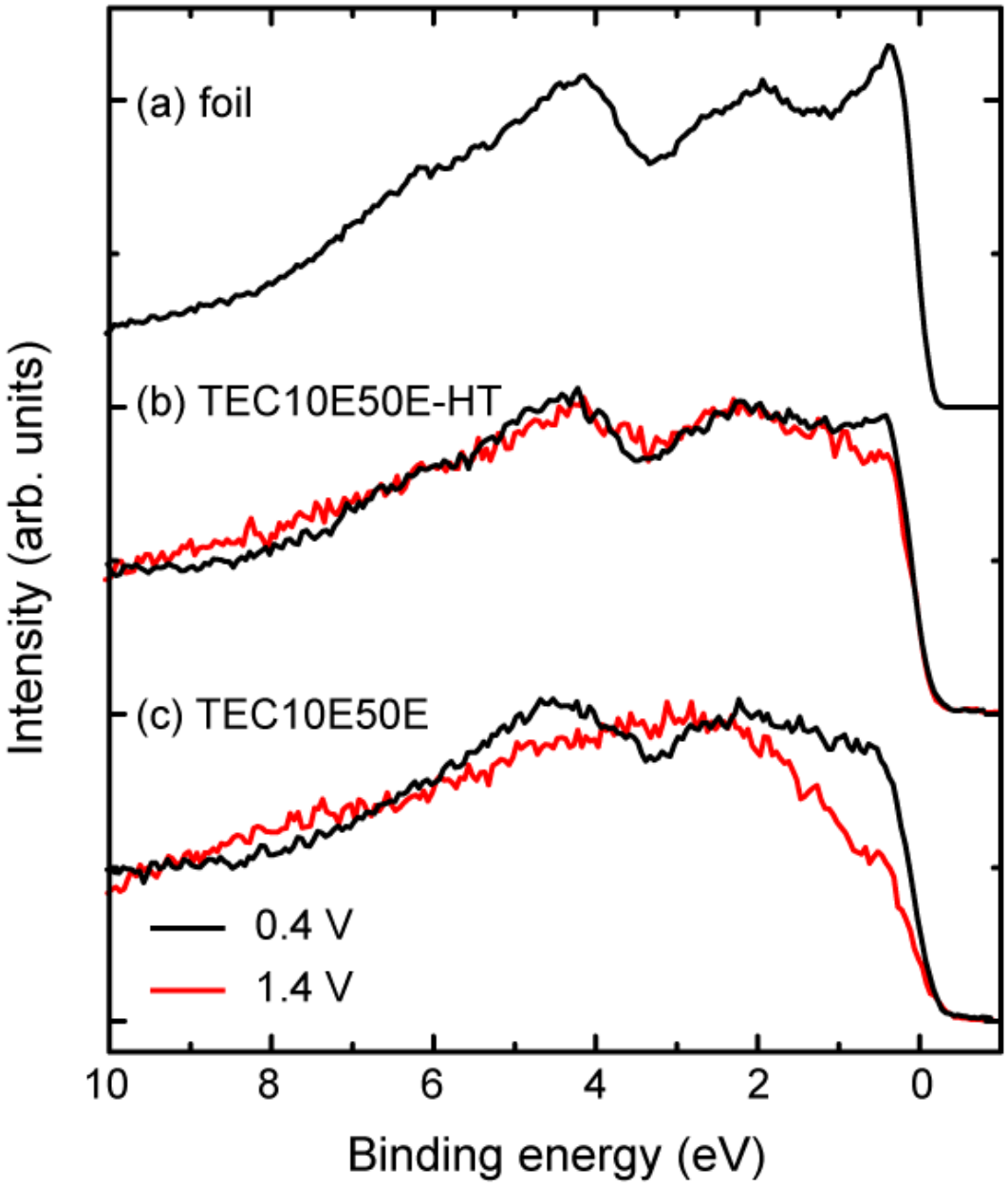
(a) foil
(b) TEC10E50E-HT
(c) TEC10E50E
0.4 V
1.4 V
Intensity (arb. units)
10
8
6
4
2
0
Binding energy (eV)

Supporting Information

In situ study of oxidation states of platinum nanoparticles on a polymer electrolyte fuel cell electrode by near ambient pressure hard X-ray photoelectron spectroscopy

Yasumasa Takagi,[*a,b] Heng Wang,[a‡] Yohei Uemura,[a,b] Takahiro Nakamura,[a] Liwei Yu,[a] Oki Sekizawa,[c] Tomoya Uruga,[c,d] Mizuki Tada,[e] Gabor Samjeskè,[c] Yasuhiro Iwasawa,[c] and Toshihiko Yokoyama[a,b]

[a] Department of Materials Molecular Science, Institute for Molecular Science, Okazaki, Aichi 444-8585, Japan.

[b] SOKENDAI (The Graduate University for Advanced Studies), Okazaki, Aichi 444-8585, Japan.

[c] Innovation Research Center for Fuel Cells, The University of Electro-Communications, Chofu, Tokyo 182-8585, Japan.

[d] Japan Synchrotron Radiation Research Institute, SPring-8, Sayo, Hyogo 679-5198, Japan.

[e] Research Center for Materials Science, Nagoya University, Nagoya, Aichi 464-8602, Japan.

[‡] Present address: School of Material and Chemical Engineering, Zhengzhou University of Light Industry, Zhengzhou Henan Province, 450001, China.

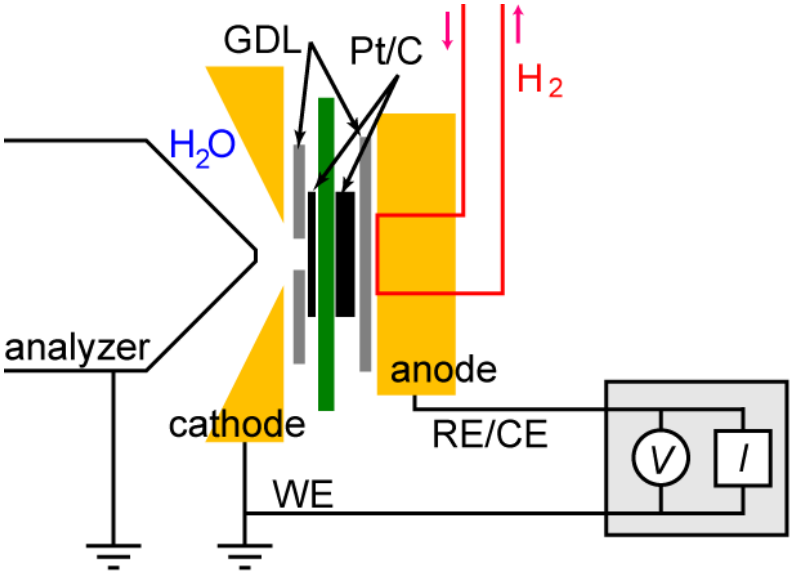

Figure S1: A potentiostatic system of the fuel cell for *in situ* NAP-HAXPES measurements at SPring-8 BL36XU.

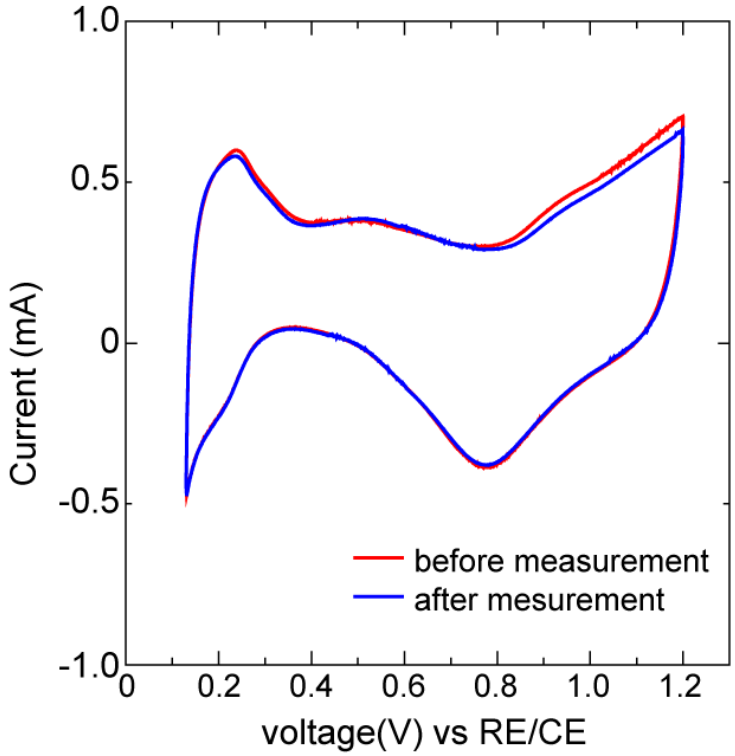

Figure S2: Cyclic voltammograms before and after the *in situ* NAP-HAXPES measurement for 4 hours under water vaper pressure of 4,000 Pa. The scan rate of the CV curves was 20 mV/s. TEC10E50E was used as the catalyst in the electrode.